# Functional modulation of IFT kinesins extends the sensory repertoire of ciliated neurons in *Caenorhabditis elegans*

James E. Evans,[1] Joshua J. Snow,[1] Amy L. Gunnarson,[1] Guangshuo Ou,[1] Henning Stahlberg,[1] Kent L. McDonald,[2] and Jonathan M. Scholey[1]

[1]Section of Molecular and Cellular Biology, University of California, Davis, Davis, CA 95616
[2]Electron Microscopy Laboratory, University of California, Berkeley, Berkeley, CA 94720

The diversity of sensory cilia on *Caenorhabditis elegans* neurons allows the animal to detect a variety of sensory stimuli. Sensory cilia are assembled by intraflagellar transport (IFT) kinesins, which transport ciliary precursors, bound to IFT particles, along the ciliary axoneme for incorporation into ciliary structures. Using fluorescence microscopy of living animals and serial section electron microscopy of high pressure–frozen, freeze-substituted IFT motor mutants, we found that two IFT kinesins, homodimeric OSM-3 kinesin and heterotrimeric kinesin II, function in a partially redundant manner to build full-length amphid channel cilia but are completely redundant for building full-length amphid wing (AWC) cilia. This difference reflects cilia-specific differences in OSM-3 activity, which serves to extend distal singlets in channel cilia but not in AWC cilia, which lack such singlets. Moreover, AWC-specific chemotaxis assays reveal novel sensory functions for kinesin II in these wing cilia. We propose that kinesin II is a "canonical" IFT motor, whereas OSM-3 is an "accessory" IFT motor, and that subtle changes in the deployment or actions of these IFT kinesins can contribute to differences in cilia morphology, cilia function, and sensory perception.

## Introduction

Cilia are remarkable microtubule (MT)-based "nanomachines" that project from the surface of most eukaryotic cells and play diverse roles in motility and sensory reception (Rosenbaum and Witman, 2002; Pazour and Witman, 2003; Scholey, 2003; Snell et al., 2004). Sensory cilia on the dendritic endings of chemosensory neurons in *Caenorhabditis elegans* act as sensory antennae that control the animal's chemotactic movements in response to chemical gradients in the environment (Perkins et al., 1986). These cilia have distinct neuron-specific morphologies and sense different chemical stimuli (Bargmann et al., 1993; Lanjuin and Sengupta, 2004). For example, although the amphid channel cilia have a typical unbranched cylindrical morphology and detect hydrophilic molecules and high osmolarity, the adjacent amphid wing (AWC) cilia have a fan-like morphology and detect volatile odorants (e.g., benzaldehyde; Fig. 1; Perkins et al., 1986; Lanjuin and Sengupta, 2004). How these distinct structures and sensory modalities arise is unclear, although differences in intraflagellar transport (IFT) motor function in different cilia could play a key role.

IFT motors of the kinesin 2 family (Lawrence et al., 2004) assemble and maintain cilia by transporting ciliary precursors, bound to multimeric protein complexes called IFT particles, from the cell body, along the axoneme, for incorporation into ciliary structures (Rosenbaum and Witman, 2002; Cole, 2003; Scholey, 2003). In some organisms, a single heterotrimeric kinesin 2 motor transports the IFT particles to the distal tip of the cilium, and a second motor, IFT dynein, recycles kinesin 2, IFT particles, and turnover products back to the cell body (Cole et al., 1993, 1998; Kozminski et al., 1993, 1995; Morris and Scholey, 1997; Pazour et al., 1999; Porter et al., 1999; Signor et al., 1999a). In *C. elegans* amphid channel cilia, however, two kinesin 2 motors, heterotrimeric kinesin II and homodimeric OSM-3 kinesin, cooperate in a semiredundant fashion to build two distinct domains of the axoneme: the middle segment consisting of nine MT doublets surrounding a few central singlets and the distal segment consisting of MT singlets, which are extensions of the middle segment A tubules (Fig. 1; Orozco et al., 1999; Signor et al., 1999b; Snow et al., 2004; Ou et al., 2005).

Correspondence to Jonathan M. Scholey: jmscholey@ucdavis.edu

Abbreviations used in this paper: 3D, three-dimensional; AWC, amphid wing; IFT, intraflagellar transport; MT, microtubule; RFP, red fluorescent protein; TEM, transmission EM; WT, wild type.

The online version of this article contains supplemental material.


The Journal of Cell Biology, Vol. 172, No. 5, February 27, 2006 663–669
http://www.jcb.org/cgi/doi/10.1083/jcb.200509115

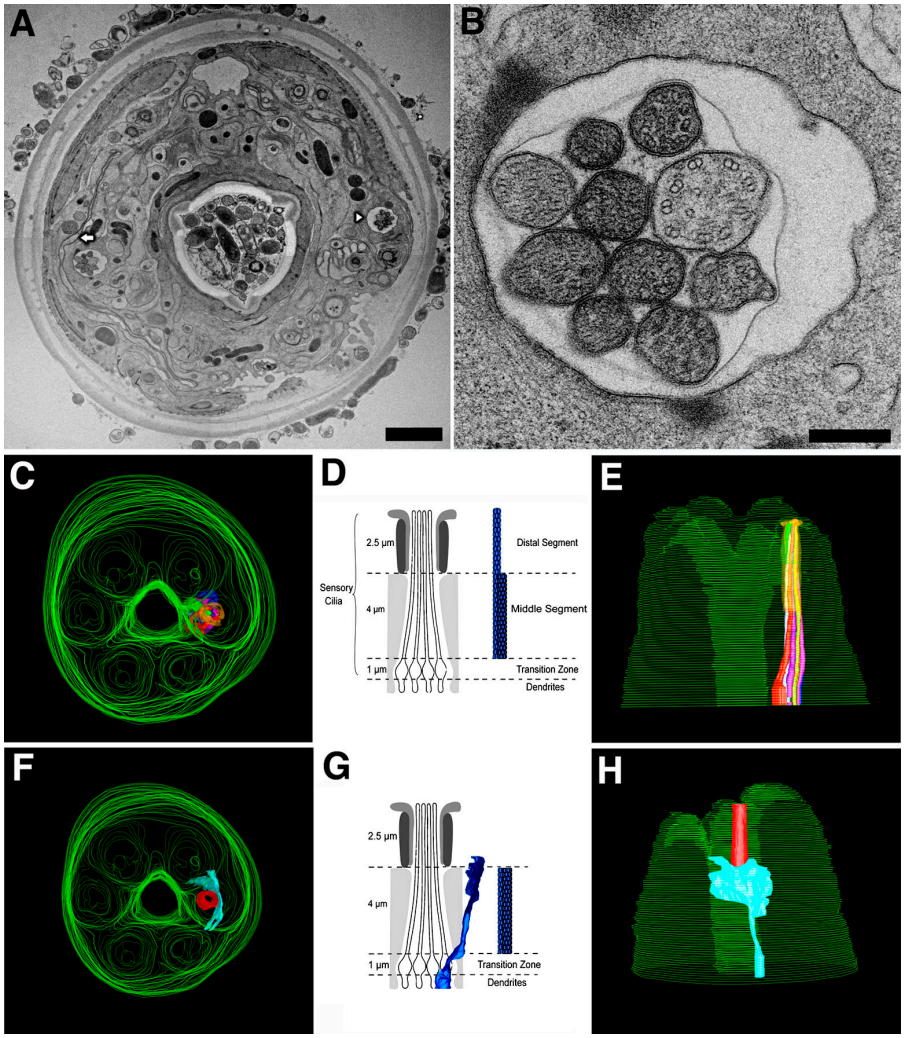


Figure 1. **TEM analysis of the head of WT *C. elegans*.** (A) Micrograph of a section of WT *C. elegans* ~5 µm from the tip of the head. Bar, 2 µm. The arrowhead marks the amphid channel cilia, and the arrow depicts the AWC. (B) Enlargement of right amphid pore depicting the MT doublets characteristic of the middle zone. Bar, 250 nm. (C and E) Top and side views of a 3D reconstruction from aligned serial sections showing overview of head and location of amphid channel cilia. (D) Illustration of middle segment MT doublets and distal MT singlets of channel cilia. (F and H) Top and side views of a 3D reconstruction of head showing locations of AWC around amphid pore. (G) Illustration of longitudinal section through fan-like AWC cilium adjacent to amphid channel cilia. The middle segments of channel and AWC cilia both contain doublets and singlets. In channel cilia, these MTs maintain a cylindrical morphology, but in AWC they "splay apart" laterally and end together ~0.5 µm below the distal membrane (i.e., AWC doublet A tubules do not extend distal singlets).

(We use the standard name, kinesin 2, to describe the family and the terms kinesin II and OSM-3 kinesin to discriminate the two *C. elegans* IFT kinesin holoenzymes.) The two motors move the same IFT particles along the middle segment in a process that is required to build the middle segment, and then OSM-3 kinesin alone moves them the rest of the way along the distal segment in a process that is required to elongate the distal singlets.

Therefore, in *C. elegans*, the basic "canonical" mechanism of IFT, in which a single anterograde motor delivers precursors to the tip of the assembling cilium, is complicated by the use of two kinesin 2 motors, but what selective advantage might this confer? We address the possibility that the differential regulation of the two motors in different cilia may contribute to neuron-specific sensory ciliary diversity. We reconstructed the three-dimensional (3D) structure of the cilia from serial EM sections of wild type (WT), kinesin II (*klp-11*, *kap-1*), OSM-3 kinesin (*osm-3*), and kinesin II/OSM-3 (*osm-3;klp-11* and *osm-3; kap-1*) single- and double-mutant animals. To ensure optimal preservation of cell ultrastructure, worms were high-pressure frozen and freeze substituted (Muller-Reichert et al., 2003). The results confirm our model in which OSM-3 and kinesin II function redundantly to build the middle segments of amphid channel cilia, whereas OSM-3 alone builds the distal singlets (Snow et al., 2004), but suggest that, in the adjacent fan-like AWC cilia, the kinesin 2 motors have a different functional relationship that appears to contribute to the morphological and sensory differences between the AWC and channel cilia.

## Results and discussion

### Partially redundant roles of IFT kinesins in building amphid channel cilia

Fig. 1 shows the general organization of the head of an adult *C. elegans* as revealed by transmission EM (TEM) of high pressure–frozen, freeze-substituted WT animals and 3D reconstructions from serial sections. We observed excellent preservation of the animal's fine structure, including obvious MT doublets and singlets of the cilia (Fig. 1, A and B). In the middle segments, nine doublet MTs surround a variable number of singlets, characteristic of immotile cilia (Fig. 1 B). We consistently observed that the matrix of some cilia was more intensely stained than others, possibly reflecting a larger number of electron-dense IFT particles (Fig. 1 B; Kozminski et al., 1993). In the reconstructions, the hexaradiate symmetry of the head is obvious (Fig. 1, C and F), and in each of the two amphids, 10 cilia form a bundle that extends to the tip of the channel (Fig. 1 E), whereas the

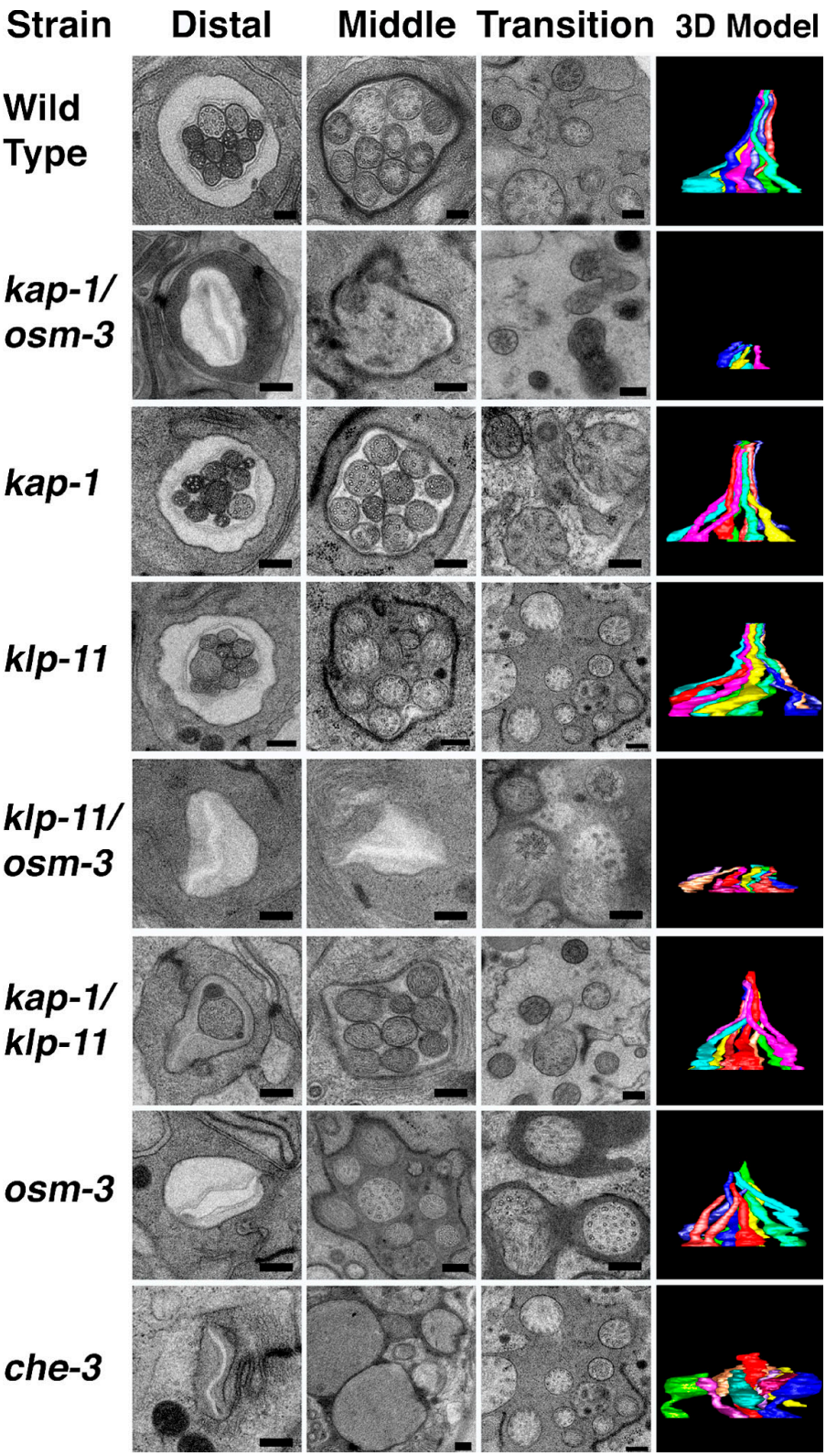


Figure 2. **TEM analysis of amphid channel cilia in IFT motor mutants.** Representative micrographs of distal and middle segments and transition zones and a side view of the corresponding 3D model that was reconstructed from serial sections from each strain. 3D reconstructions show trajectories of channel cilia obtained from serial sections taken from the distal tip at the amphid pore down through the basal transition zones to the dendrites (total length ~10 μm). Bars, 250 nm.

fan-shaped AWC cilium does not enter the channel but instead penetrates the adjacent sheath and socket cells.

We reconstructed amphid channel cilia from WT animals and from a variety of IFT motor mutants (Fig. 2) and observed that in WT animals and single (*kap-1* and *klp-11*) and double (*kap-1;klp-11*) kinesin II mutants, full-length cilia, ~7.5 μm in length, were present. In mutants lacking IFT dynein function (*che-3*), the cilia are truncated and bulbous, whereas cilia in mutants lacking OSM-3 kinesin function (*osm-3*) were only 4.5 μm long because of the specific loss of distal segments

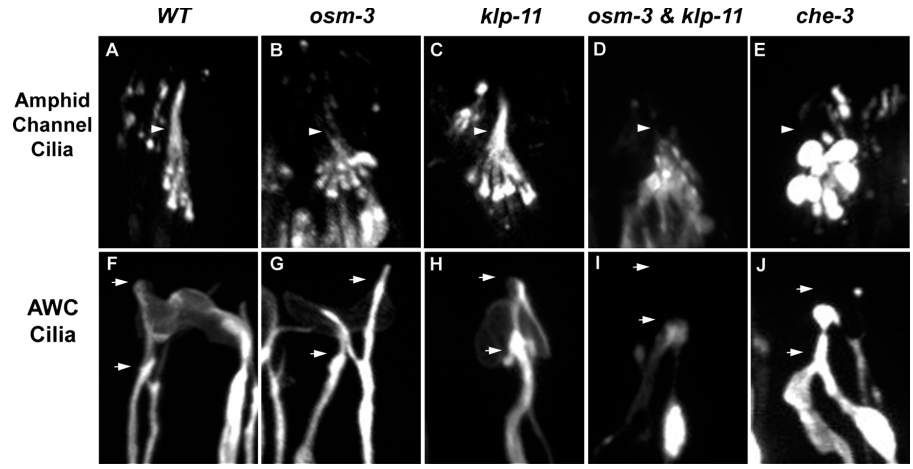


Figure 3. **Fluorescence microscopy of amphid channel cilia and AWC cilia in IFT motor mutants.** (A–E) Amphid channel cilia visualized with IFT particle proteins, OSM-5::GFP (A, B, and E), or OSM-6::GFP (C and D). (A) Channel cilia in WT (*7.5* μm full length); (B) *osm-3* mutant missing 2.5 μm distal segments; (C) *klp-11* mutants have intact cilia; (D) *osm-3;klp-11* double mutants lacking entire axoneme; (E) *che-3* mutant cilia deformed into bulbous endings. Arrowheads indicate middle (bottom) and distal (top) segment boundaries. (F–J) AWC cilia labeled with the AWC guanylyl cyclase, ODR-1::RFP. (F) The flattened ciliated endings of AWC neuron in WT. (G and H) AWC cilia of *osm-3* (G) or *klp-11* (H) mutants are indistinguishable from WT. (I) *osm-3;klp-11* double mutants completely lack AWC cilia and form aggregates in the dendrites. (J) In *che-3* mutants, ciliary endings contain bulbous aggregates. Arrows indicate positions of proximal and distal ends of branched, forked, WT AWC cilia.

(Perkins et al., 1986). In OSM-3 kinesin/kinesin II double mutants (*kap-1;osm-3* and *klp-11;osm-3*), however, the entire ciliary axoneme was missing (Fig. 2). In previous work, we observed no fluorescent IFT particles (GFP::OSM-6) extending from the transition zone of these double mutants (Snow et al., 2004). Our TEM analysis rigorously eliminates the possibility that this reflected a failure of transport of IFT particles along residual cilia in these animals (assembled, for example, by diffusion of ciliary precursors to their site of assembly) but instead is due to a complete loss of ciliary axonemes, confirming that either OSM-3 kinesin or kinesin II is required to build the middle segments of these axonemes, whereas OSM-3 alone is required to extend the distal singlets (Perkins et al., 1986; Snow et al., 2004).

### Redundant roles of IFT kinesins in building AWC cilia

Although kinesin II and OSM-3 kinesin act in a partially redundant fashion to build the channel ciliary axonemes, they act in a completely redundant fashion to build the adjacent AWC cilia (Figs. 3–5). We used fluorescence microscopy (Fig. 3) to examine the distribution of GFP-tagged translational reporters of IFT particle proteins (OSM-5 or OSM-6::GFP) in amphid channel cilia and a red fluorescent protein (RFP)–tagged transcriptional reporter of the AWC guanylyl cyclase ODR-1::RFP (L'Etoile and Bargmann, 2000) to examine the morphology of AWC cilia. The channel and wing cilia in WT animals (Fig. 3, A and F) were indistinguishable from those in single mutants in the kinesin II motor (Fig. 3, C and H). However, although the apparent lengths of the channel cilia in *osm-3* mutants were reduced from 7.5 to 5 μm because of the loss of their distal segments (Fig. 3 B), the morphology of wing cilia was indistinguishable from WT (compare Fig. 3, F and G). No differences in the morphology of any single mutant and WT AWC cilia could be detected by visual inspection of scores of animals. Our efforts to quantify the dimensions of these AWC cilia yielded equivocal results. The largest measured difference was between WTs (length, 5.04 ± 1.08 μm, and width, 8.9 ± 2.16 μm; $n = 32$) and *klp-11* (length, 4.56 ± 0.98 μm, and width, 8.62 ± 1.92 μm; $n = 33$), but this small difference probably results from problems encountered in tracking fluorescence from edge to edge along these asymmetric cilia. However, clear and obvious differences were noted in kinesin II/OSM-3 kinesin double mutants (*klp-11;osm-3*), where no fluorescence was observed distal to the transition zone, consistent with a complete loss of cilia on the AWC neuron (Fig. 3 I). We confirmed that kinesin II and OSM-3 kinesin are indeed expressed in AWC neurons because translational fusions of KAP-1::GFP (Fig. 4 A) and OSM-3::GFP (Fig. 4 B) colocalized with the AWC marker, ODR-1::RFP (Fig. 4, A and B). The results suggest that either kinesin II or OSM-3 kinesin can build the AWC cilia and that either motor, but not both, is dispensable for this. No differences in IFT dynein function were seen, based on the morphology of channel and AWC cilia (Fig. 3, E and J).

We used serial-section TEM to confirm that the morphology defects seen in AWC cilia by light microscopy of the IFT motor mutants reflect changes in ciliary structure (Fig. 5). By examining multiple serial sections, we found that AWC cilia were intact in WT and in single kinesin II or OSM-3 mutants but were completely absent in double mutants (Fig. 5). Careful examination of WT cilia revealed mixtures of doublet and singlet MTs that lie side by side rather than being organized into a cylinder (Fig. 5 A, insets). Significantly, moving toward the distal tip of the cilium, both the singlet and doublet MTs terminated at the same point, ∼0.5 μm below the overlying ciliary membrane. Because serial sections were taken every 100 nm, the maximum length of any distal singlets must be less than this distance (i.e., 1/25 the length of the distal singlets in channel cilia), suggesting that AWC cilia lack distal singlets. Therefore,

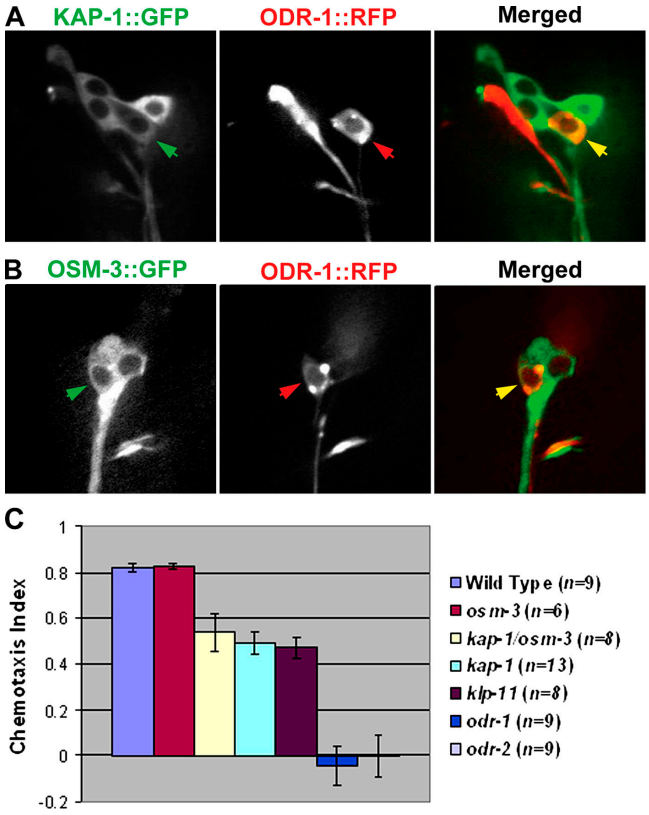


Figure 4. **Expression and function of kinesin II and OSM-3 kinesin in AWC neurons.** (A and B) Kinesin II (KAP-1::GFP, A) and OSM-3 kinesin (OSM-3::GFP, B) colocalize with an AWC marker, ODR-1::RFP. (left) KAP-1::GFP (A, green) or OSM-3::GFP (B, green); (middle) ODR-1::RFP (red); (right) merged images (yellow). Arrows point to the cell bodies of AWC neurons in which kinesin 2 motors colocalize with the AWC marker. (C) Chemotaxis toward benzaldehyde by WT, OSM-3 kinesin, and kinesin II mutants. *klp-11;osm-3* double mutants could not be assayed because their movement was very sluggish because of the presence of the *dumpy* marker that was introduced in the genetic crosses (see Materials and methods). Error bars represent SEM.

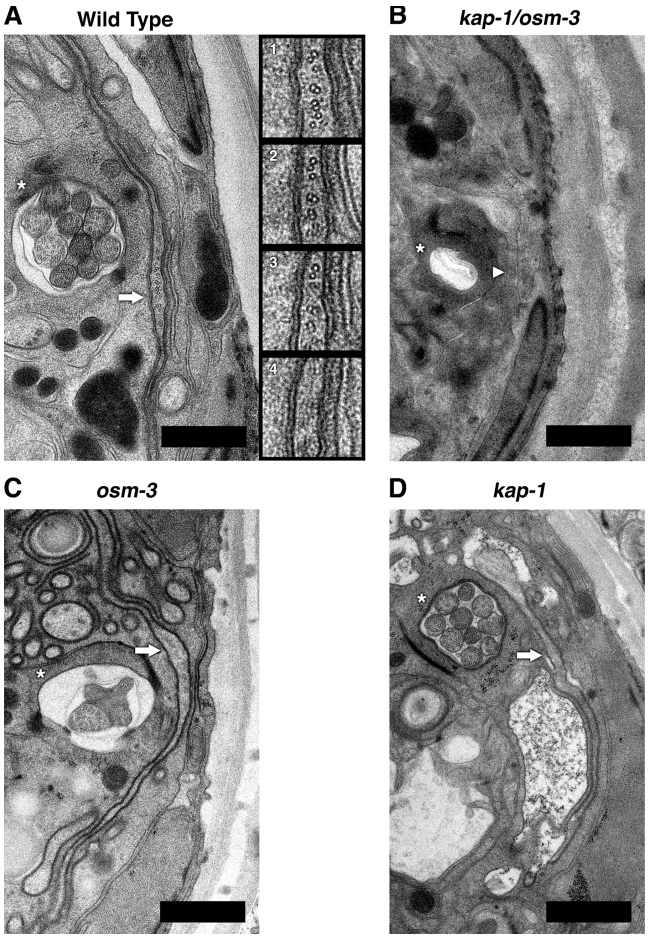


Figure 5. **TEM analysis of the AWC in WT and IFT motor mutant animals.** (A) Electron micrograph of amphid channel containing 10 channel cilia and the fan-like AWC cilium from WT *C. elegans*. Inset 1 is a 5× magnification of the AWC (A, arrow) showing mixed MT doublets and singlets. Insets 2–4 show consecutive serial sections moving toward the distal tip of the cilium. Note that doublets and singlets are present in section 3 and absent in section 4, showing that they end abruptly. (B) Micrograph depicting the empty and collapsed amphid pore from the *kap-1;osm-3* double mutant also lacking the AWC cilium. (C and D) Intact AWC cilia are also present in *osm-3* and *kap-1* single mutants. Within each micrograph, a single amphid pore is indicated by an asterisk, and a single AWC cilium is marked either by a solid arrow, if it has a normal fan-like structure, or by an arrowhead, to indicate the absence of the AWC cilium. Bars, 1 μm.

the two motors act redundantly to build the doublet and singlet MTs of AWC cilia just like in the middle segments of channel cilia, whereas OSM-3 extends the distal singlets in channel cilia but not in AWC cilia, where its function is unknown.

Why channel cilia require distal singlets whereas AWC cilia do not is unclear, and in general the function of distal segments is unknown. The distal segments of cilia and flagellar axonemes in other systems are of variable length and prominence; e.g., they are 200 μm long in frog olfactory cilia (Reese, 1965), whereas in *Chlamydomonas reinhardtii* they are lacking, but they do elongate transiently during mating (Mesland et al., 1980). There are speculations that distal singlets are dynamic structures that are required for some aspect of sensory signaling because the specific loss of the singlets (e.g., in *osm-3* mutants) leads to loss of sensory signaling. However, both the channel and wing cilia have sensory functions in *C. elegans*, so this may not be universally true.

Based on studies of amphid channel cilia (Snow et al., 2004), we had predicted that OSM-3 kinesin would be deployed in a broad range of cilia to specifically elongate the distal singlets. However, the current study suggests that this is an oversimplification because AWC cilia in WTs do not have distal singlets and these cilia were morphologically indistinguishable in *osm-3* mutants and WTs. It will now be interesting to identify regulatory factors that act via OSM-3 to control the elongation of the distal singlets either by promoting their extension in channel cilia or by suppressing their extension in wing cilia. Such factors may be uncovered among ciliary mutants (Perkins et al., 1986; Starich et al., 1995; Ou et al., 2005).

## Novel chemosensory function for kinesin II in AWC cilia

Sensory cilia in the head of the animal have diverse functions and provide diverse sensory modalities. Defects in osmotic avoidance are associated with the channel cilia and are present in *osm-3* mutants but not in *klp-11* or *kap-1* mutants (Snow et al., 2004). We used chemotaxis toward benzaldehyde as a specific assay for AWC cell function (Fig. 4 C; Bargmann et al., 1993) and

observed that chemotaxis was normal in WT animals and in *osm-3* mutants, but in *klp-11* or *kap-1* single and *osm-3;kap-1* double mutants, chemotaxis was impaired by ~50%, similar to the IFT particle mutant, *osm-1* (Peckol et al., 1999). The results suggest that these two motors are functionally redundant for AWC ciliary length determination, but once a full-length cilium is assembled, kinesin II has additional chemosensory functions that may involve the delivery of signaling molecules for incorporation into cilia, as proposed for *C. reinhardtii* kinesin II (Pan and Snell, 2002). Future studies of ciliary mutants may uncover this predicted cargo of kinesin II.

How kinesin II and OSM-3 redundantly assemble AWC cilia is unclear because we were unable to detect IFT in assays identical to those that demonstrate vigorous IFT along channel cilia (Snow et al., 2004; Ou et al., 2005). Thus, it is possible that in AWC neurons, ciliary assembly does not depend on IFT and the kinesin 2 motors build cilia using a different mechanism. However, we favor the idea that IFT does operate in these cilia but was not seen because it occurs transiently during de novo ciliary assembly or for technical reasons such as a low level of expression of the IFT machinery.

Thus, in the simple, canonical mechanism of IFT, kinesin II alone delivers precursors to the tip of assembling cilia to build the axoneme. In *C. elegans* and perhaps elsewhere, OSM-3 is deployed as an "accessory" motor to functionally substitute for the loss of kinesin II function or, when kinesin II is active, to augment the canonical IFT pathway and, in some cases, to elongate the distal singlets. Our results suggest that modulating the activity of the two IFT kinesins in different cilia contributes to functional differences between cilia on different sensory neurons, providing a selective advantage by allowing the animal to receive and respond to a greater diversity of sensory cues.

## Materials and methods

### Genetic crosses

Animals were maintained and crossed using standard methods (Brenner, 1974) as described previously (Snow et al., 2004). Homozygosity was confirmed for *osm-3(p802)IV* and *che-3(e1124)I* by dye filling and for *kap-1 (ok676)III* and *klp-11(tm324)IV* by single-worm PCR. Because *klp-11* and *osm-3* are on the same chromosome, we crossed *klp-11(tm324)IV;dpy-20(e1282)IV* with *osm-3 (p802)IV;mnIs17[osm-6::gfp]* to produce animals with the final genotype *klp-11(tm324)IV;dpy-20(e1282)IV;osm-3 (p802)IV;mnIs17[osm-6::gfp]*. Amphid channel cilia were marked by introducing either *mnIs17[osm-6::gfp]* or *Ex[osm-5::gfp + rol-6(su1006)]* into motor mutants, and AWC cilia in WT and mutants were imaged with oyIs44[*odr-1::rfp*]. ODR-1::RFP was supplied by P. Sengupta (Brandeis University, Waltham, MA).

### Fluorescence microscopy

As described previously (Snow et al., 2004; Ou et al., 2005), worms were anesthetized with 10 mM levamisole, mounted on agar pads, and maintained at 21°C. Fluorescent images were collected on a microscope (Olympus) equipped with a 100×, 1.35 NA objective and a spinning disc confocal head (UltraView; PerkinElmer) and further processed using MetaMorph software (Universal Imaging Corp.).

### TEM and image processing

Specimens were ultrarapidly frozen using a high-pressure freezer (HPM 010; Bal-Tec) and freeze substituted at −90°C in anhydrous acetone containing 1% osmium tetroxide and 0.1% uranyl acetate using an EM AFS (Leica; Muller-Reichert et al., 2003). The cryofixed specimens were raised to room temperature and subsequently infiltrated and embedded in Epon-Araldite resin. Samples were cut into 100-nm-thick sections using an Ultracut E microtome (Leica). Serial sections were collected on slot grids covered with a Formvar support film, poststained with 2% uranyl acetate followed by Reynold's lead citrate, and covered by a second layer of Formvar for increased stability. Grids were visualized on a transmission electron microscope (JEM-2100FEG; JEOL) operated at 200 keV. Images of each section were recorded at ~4 μm defocus on a 4,096 × 4,096–pixel charge-coupled device camera (Tietz; TVIPS) and at a nominal magnification of 8,000, yielding a pixel size of 1.25 nm. The images of the serial sections were manually aligned using the manual image deformation and alignment system (Mastronarde et al., 1992) and modeled as surface renderings using 3DMOD to depict the length and paths of the amphid pore and each cilium (Kremer et al., 1996).

### Chemotaxis assays

Chemotaxis assays were performed as described previously (Bargmann et al., 1993). 15–20 young adult animals were placed onto a 10-cm Petri dish without bacteria for 1 h and then transferred to a 10-cm Petri dish containing 1.6% Bacto agar, 5 mM potassium phosphate, pH 6.0, 1 mM $CaCl_2$, and 1 mM $MgSO_4$, along with 2 μl of the attractant, benzaldehyde (1:200 in ethanol), and 2 μl of the counterattractant, ethanol. The worms were placed at a marked origin, equidistant from the attractant and counterattractant, 2 μl of sodium azide was used to anesthetize the animals, and the numbers located at attractant and counterattractant were counted after 1 h. The chemotaxis index was defined as follows: (numbers at attractant − numbers at counterattractant) ÷ total (Peckol et al., 1999). Assays were repeated multiple times. A one-way analysis of variance was performed using Proc Mixed (SAS Institute), and obvious assay differences between strains were observed using Tukey's test for multiple comparisons at a significance level of 0.05. On the graphs (Fig. 4 C), standard error bars are shown.

### Online supplemental material

Fig. S1 shows a transmission electron micrograph of sections of each strain ~5 μm from the tip of the head. Online supplemental material is available at http://www.jcb.org/cgi/content/full/jcb.200509115/DC1.

We thank Piali Sengupta for discussions on amphid cilia and Noelle L'Etoile for advice on chemotaxis assays.

This research was supported by a grant from the National Institutes of Health (GM50718) to J.M. Scholey.

Submitted: 20 September 2005
Accepted: 24 January 2006

## References

Bargmann, C.I., E. Hartwieg, and H.R. Horvitz. 1993. Odorant-selective genes and neurons mediate olfaction in *C. elegans*. *Cell.* 74:515–527.

Brenner, S. 1974. The genetics of *Caenorhabditis elegans*. *Genetics.* 77:71–94.

Cole, D.G. 2003. The intraflagellar transport machinery of *Chlamydomonas reinhardtii*. *Traffic.* 4:435–442.

Cole, D.G., S.W. Chinn, K.P. Wedaman, K. Hall, T. Vuong, and J.M. Scholey. 1993. Novel heterotrimeric kinesin-related protein purified from sea urchin eggs. *Nature.* 366:268–270.

Cole, D.G., D.R. Diener, A.L. Himelblau, P.L. Beech, J.C. Fuster, and J.L. Rosenbaum. 1998. *Chlamydomonas* kinesin-II-dependent intraflagellar transport (IFT): IFT particles contain proteins required for ciliary assembly in *Caenorhabditis elegans* sensory neurons. *J. Cell Biol.* 141:993–1008.

Kozminski, K.G., K.A. Johnson, P. Forscher, and J.L. Rosenbaum. 1993. A motility in the eukaryotic flagellum unrelated to flagellar beating. *Proc. Natl. Acad. Sci. USA.* 90:5519–5523.

Kozminski, K.G., P.L. Beech, and J.L. Rosenbaum. 1995. The *Chlamydomonas* kinesin-like protein FLA10 is involved in motility associated with the flagellar membrane. *J. Cell Biol.* 131:1517–1527.

Kremer, J.R., D.N. Mastronarde, and J.R. McIntosh. 1996. Computer visualization of three-dimensional image data using IMOD. *J. Struct. Biol.* 116:71–76.

Lanjuin, A., and P. Sengupta. 2004. Specification of chemosensory neuron subtype identities in *Caenorhabditis elegans*. *Curr. Opin. Neurobiol.* 14:22–30.

Lawrence, C.J., R.K. Dawe, K.R. Christie, D.W. Cleveland, S.C. Dawson, S.A. Endow, L.S. Goldstein, H.V. Goodson, N. Hirokawa, J. Howard, et al. 2004. A standardized kinesin nomenclature. *J. Cell Biol.* 167:19–22.

L'Etoile, N.D., and C.I. Bargmann. 2000. Olfaction and odor discrimination are mediated by the *C. elegans* guanylyl cyclase ODR-1. *Neuron.* 25:575–586.

Mastronarde, D.N., E.T. O'Toole, K.L. McDonald, J.R. McIntosh, and M.E. Porter. 1992. Arrangement of inner dynein arms in wild-type and mutant flagella of *Chlamydomonas*. *J. Cell Biol.* 118:1145–1162.

Mesland, D.A., J.L. Hoffman, E. Caligor, and U.W. Goodenough. 1980. Flagellar tip activation stimulated by membrane adhesions in *Chlamydomonas* gametes. *J. Cell Biol.* 84:599–617.

Morris, R.L., and J.M. Scholey. 1997. Heterotrimeric kinesin-II is required for the assembly of motile 9+2 ciliary axonemes on sea urchin embryos. *J. Cell Biol.* 138:1009–1022.

Muller-Reichert, T., H. Hohenberg, E.T. O'Toole, and K. McDonald. 2003. Cryoimmobilization and three-dimensional visualization of *C. elegans* ultrastructure. *J. Microsc.* 212:71–80.

Orozco, J.T., K.P. Wedaman, D. Signor, H. Brown, L. Rose, and J.M. Scholey. 1999. Movement of motor and cargo along cilia. *Nature.* 398:674.

Ou, G., O.E. Blacque, J.J. Snow, M.R. Leroux, and J.M. Scholey. 2005. Functional coordination of intraflagellar transport motors. *Nature.* 436:583–587.

Pan, J., and W.J. Snell. 2002. Kinesin-II is required for flagellar sensory transduction during fertilization in *Chlamydomonas*. *Mol. Biol. Cell.* 13:1417–1426.

Pazour, G.J., and G.B. Witman. 2003. The vertebrate primary cilium is a sensory organelle. *Curr. Opin. Cell Biol.* 15:105–110.

Pazour, G.J., B.L. Dickert, and G.B. Witman. 1999. The DHC1b (DHC2) isoform of cytoplasmic dynein is required for flagellar assembly. *J. Cell Biol.* 144:473–481.

Peckol, E.L., J.A. Zallen, J.C. Yarrow, and C.I. Bargmann. 1999. Sensory activity affects sensory axon development in *C. elegans*. *Development.* 126:1891–1902.

Perkins, L.A., E.M. Hedgecock, J.N. Thomson, and J.G. Culotti. 1986. Mutant sensory cilia in the nematode *Caenorhabditis elegans*. *Dev. Biol.* 117:456–487.

Porter, M.E., R. Bower, J.A. Knott, P. Byrd, and W. Dentler. 1999. Cytoplasmic dynein heavy chain 1b is required for flagellar assembly in *Chlamydomonas*. *Mol. Biol. Cell.* 10:693–712.

Reese, T.S. 1965. Olfactory cilia in the frog. *J. Cell Biol.* 25:209–230.

Rosenbaum, J.L., and G.B. Witman. 2002. Intraflagellar transport. *Nat. Rev. Mol. Cell Biol.* 3:813–825.

Scholey, J.M. 2003. Intraflagellar transport. *Annu. Rev. Cell Dev. Biol.* 19:423–443.

Signor, D., K.P. Wedaman, J.T. Orozco, N.D. Dwyer, C.I. Bargmann, L.S. Rose, and J.M. Scholey. 1999a. Role of a class DHC1b dynein in retrograde transport of IFT motors and IFT raft particles along cilia, but not dendrites, in chemosensory neurons of living *Caenorhabditis elegans*. *J. Cell Biol.* 147:519–530.

Signor, D., K.P. Wedaman, L.S. Rose, and J.M. Scholey. 1999b. Two heteromeric kinesin complexes in chemosensory neurons and sensory cilia of *Caenorhabditis elegans*. *Mol. Biol. Cell.* 10:345–360.

Snell, W.J., J. Pan, and Q. Wang. 2004. Cilia and flagella revealed: from flagellar assembly in *Chlamydomonas* to human obesity disorders. *Cell.* 117:693–697.

Snow, J.J., G. Ou, A.L. Gunnarson, M.R. Walker, H.M. Zhou, I. Brust-Mascher, and J.M. Scholey. 2004. Two anterograde intraflagellar transport motors cooperate to build sensory cilia on *C. elegans* neurons. *Nat. Cell Biol.* 6:1109–1113.

Starich, T.A., R.K. Herman, C.K. Kari, W.H. Yeh, W.S. Schackwitz, M.W. Schuyler, J. Collet, J.H. Thomas, and D.L. Riddle. 1995. Mutations affecting the chemosensory neurons of *Caenorhabditis elegans*. *Genetics.* 139:171–188.